IOP Publishing Physica Scripta
Phys. Scr. 94 (2019) 115007 (6pp) https://doi.org/10.1088/1402-4896/ab2418

Valid corollaries of polarization-separated color attributes for a multi-layer dielectric structure

Dong Qi[1], Xian Wang[1], Fu Chen[1], Honggang Gu[2], Shiyuan Liu[2] and Rongzhou Gong[1]

[1] School of Optical and Electronic Information, Huazhong University of Science and Technology, Wuhan, 430074, People's Republic of China
[2] State Key Laboratory of Digital Manufacturing Equipment and Technology, Huazhong University of Science and Technology, Wuhan, 430074, People's Republic of China

E-mail: wangx@hust.edu.cn

Received 9 January 2019, revised 9 May 2019
Accepted for publication 23 May 2019
Published 20 August 2019

Abstract

Herein, four corollaries for polarization-separated color attributes have been firstly proposed and experimentally verified based on the systematical investigations of a multi-layer dielectric structure $L/(Ge/ZnS)^3$ (L stands for surface ZnS). Specifically, for different spectra responses to surface thicknesses d_L (30, 60 and 90 nm) and incident angles θ (45°, 60° and 75°), color attributes of synthesis, s-polarization (s) and p-polarization (p) are systematically induced as: arithmetical averaging properties of luminance factors $Y_{synthesis}\% = (Y_s\% + Y_p\%)/2$ or tristimulus values (T_v) $T_{v\text{-}synthesis} = (T_{v\text{-}s} + T_{v\text{-}p})/2$; collinearity of synthetic and polarization-separated chromaticity coordinates (CCs); constant mathematic relation of $T_v(s) > T_v(p)$; synthetic CCs partial to s-polarized CCs as $d_{p\text{-}synthesis} > d_{s\text{-}synthesis}$. These corollaries can be further generalized to common dielectric multi-layer structures due to the general derivation without any restrictions of the intrinsic parameters.

Keywords: polarization separation, color attributes, multi-layer dielectric structure

(Some figures may appear in colour only in the online journal)

1. Introduction

Over the past few centuries, much effort has been directed toward the cognition of color, which can be generalized to two main fields: chemical color and structural color [1–3]. The intrinsic optical property of material (e.g. chemical chromophores from pigment) makes chemical color an indispensable component of the natural world [2]. Compared with chemical color, structural color, derived from interference, diffraction and dispersion of electromagnetic (EM) waves [4], has attracted extensive interest from the scientific community due to more efficient, dynamic and diversified control of visible light [5–7]. Meanwhile, the defined standard CIE (International Commission on Illumination) in 1931 has been widely adopted to quantify the basic information of color, such as chromaticity coordinates (CCs), tristimulus values (T_v), dominant wavelength (DW), luminance factor (LF), etc [8–10]. Up to now, mainstream research has paid much attention to the color realization of specific structures [11] or optical compatibility for multi-purpose designs [12]; however, few studies have been devoted to further research about color attributes of polarization separation for different incident angles. Therefore, it will certainly become a current and future research hotspot to effectively grasp the objective laws of rendering optical interference color for different materials, devices and optical modules of equipment.

In this work, we have systematically derived and experimentally verified four newly proposed corollaries about polarization-separated color attributes for a previously designed multi-layer structure $L/(Ge/ZnS)^3$ (shown in figure 1) [6]. Thereinto, L stands for surface ZnS [13] with different thicknesses (30 nm, 60 nm and 90 nm). The thicknesses of alternate Ge [14] and ZnS layers are d_{Ge} (610 nm) and d_{ZnS} (1193 nm), respectively. Furthermore, we have

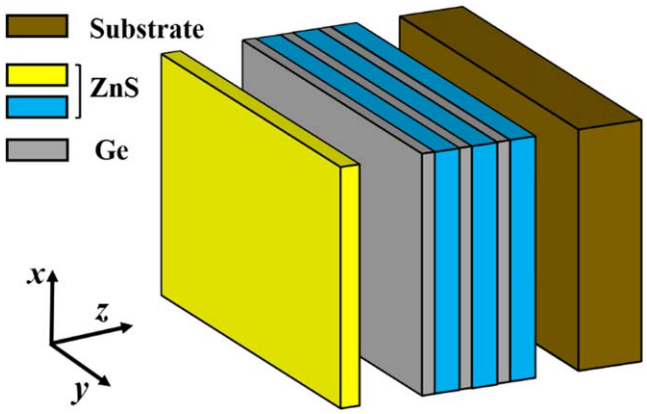

Figure 1. A schematic diagram of the designed multi-layer structure $L/(Ge/ZnS)^3$.

typically chosen off-normal 45°, 60° and 75° as original incident angles to expand the subsequent analysis. Based on the essential CIE 1931 standard [15] and an as-prepared multi-layer structure, color attributes for oblique incidence have been excavated deeply in three sub-fields LF, T_v and CCs simultaneously, which can be further subdivided into four corollaries in the next section.

2. Theoretical derivation and calculation

Actually, in order to comprehensively acquire the structural color of multi-layer dielectric films, the equal inclination interference principle has been exploited relying on constructive interference (CI) $\lambda = (2nd \cdot \cos\alpha)/m$ (m is a positive integer, α is the refraction angle, n and d are the refractive index and physical thickness, respectively) without half-wave ($\lambda/2$) loss ($n_{Air} < n_{ZnS} < n_{Ge}$) [10]. In addition, it is well-known that the CIE 1931 standard defines the color conversion from subjective cognition to objective characterization, which provides a detailed mathematical relationship among reflection spectrum $R(\lambda)$, T_v and CCs (shown in figure 2). Thereinto, T_v (X, Y and Z) can be associated with $R(\lambda)$ as a function of chromatic responses as follows:

$$X = 100\frac{\int_\lambda S(\lambda)R(\lambda)\bar{x}(\lambda)\mathrm{d}\lambda}{\int_\lambda S(\lambda)\bar{y}(\lambda)\mathrm{d}\lambda} \tag{1}$$

$$Y = 100\frac{\int_\lambda S(\lambda)R(\lambda)\bar{y}(\lambda)d\lambda}{\int_\lambda S(\lambda)\bar{y}(\lambda)d\lambda} \tag{2}$$

$$Z = 100\frac{\int_\lambda S(\lambda)R(\lambda)\bar{z}(\lambda)d\lambda}{\int_\lambda S(\lambda)\bar{y}(\lambda)d\lambda}, \tag{3}$$

where $S(\lambda)$ denotes the relative spectral power distribution of the illuminant, which is specifically adopted with artificial daylight 6500 K (D65) to accurately simulate normal circumstances. The standard observer, defined by the color-matching function values $\bar{x}$, $\bar{y}$ and $\bar{z}$, is simulated by a 10° (close observation) field of view in this work [15]. The following calculations of CCs in the chromaticity diagram are given as a function of T_v:

$$x = \frac{X}{X+Y+Z} \tag{4}$$

$$y = \frac{Y}{X+Y+Z}. \tag{5}$$

As shown in figure 2, based on fundamental definitions and the color-rendering mechanism of the multi-layer dielectric structure above, four corollaries for polarization-separated color attributes have been creatively derived with non-relevancy to the materials' intrinsic parameters (n, ε, μ, etc).

2.1. Synthetic LF (or T_v) is the mathematic average of the corresponding polarization-separated attributes.

Assuming a certain illuminant ($S(\lambda)$) and standard observer ($\bar{x}$, $\bar{y}$, $\bar{z}$), the LFs can be expressed as follows:

$$Y\% = \left(100\frac{\int_\lambda S(\lambda)R(\lambda)\bar{y}(\lambda)\mathrm{d}\lambda}{\int_\lambda S(\lambda)\bar{y}(\lambda)\mathrm{d}\lambda}\right)\%. \tag{6}$$

Substituting the constant polarization equation of reflectivity $R_{syn} = (R_s + R_p)/2$ [16], synthetic (denoted by the subscript syn) $Y\%$ can be rewritten as:

$$Y_{syn}\% = \left(100\frac{\int_\lambda S(\lambda)((R_p(\lambda) + R_s(\lambda))/2)\bar{y}(\lambda)\mathrm{d}\lambda}{\int_\lambda S(\lambda)\bar{y}(\lambda)\mathrm{d}\lambda}\right)\%. \tag{7}$$

Due to the fundamental mathematical property of the definite integration (integrating range 380–780 nm) and the approximate continuity of $\bar{x}$, $\bar{y}$, $\bar{z}$ and $S(\lambda)$ [15], equation (7) can be decomposed as follows:

$$Y_{syn}\% = \left(\frac{100}{2\cdot\int_\lambda S(\lambda)\bar{y}(\lambda)\mathrm{d}\lambda}\right)\left(\int_\lambda S(\lambda)R_p(\lambda)\bar{y}(\lambda)\mathrm{d}\lambda + \int_\lambda S(\lambda)R_s(\lambda)\bar{y}(\lambda)\mathrm{d}\lambda\right) = \frac{Y_p\% + Y_s\%}{2}. \tag{8}$$

Analogously, the mathematical derivation above can be equivalently applied to the other two $T_v\%$ ($X\%$ or $Y\%$). Therefore, it follows that:

$$X_{syn}\% = \frac{X_p\% + X_s\%}{2} \tag{9}$$

$$Z_{syn}\% = \frac{Z_p\% + Z_s\%}{2}. \tag{10}$$

Generally, the constant arithmetical averaging properties above can be directly generalized in T_v due to the identical transformation of the percent elimination. This corollary provides a quantitative criterion to analyze the mathematical relationship of the polarized color parameters LF or T_v; that

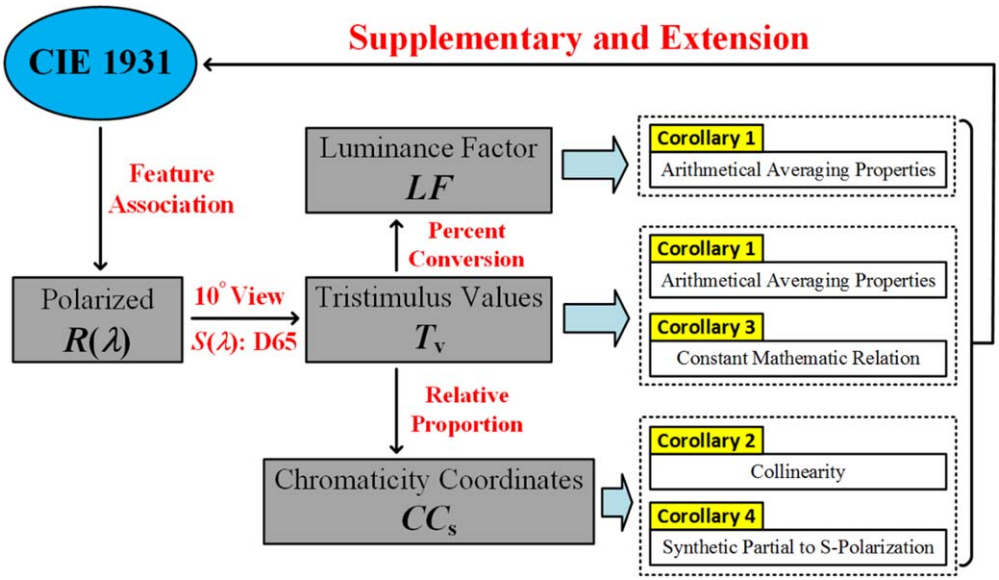

Figure 2. A schematic of the derivation process and interrelations for polarization-separated color attributes.

is, arithmetical averaging properties of T_v ($T_{v\text{-}syn} = (T_{v\text{-}s} + T_{v\text{-}p})/2$) or LF ($Y_{syn}\% = (Y_s\% + Y_p\%)/2$). To sum up, redefined three-primary colors (i.e. T_v) X (red), Y (green) or Z (blue), converted from the CIE 1931 RGB system, accurately satisfy the respective mean-value relationship of polarization-separated T_v, especially polarized color luminance. Furthermore, it indicates that actual observers can carry out specific mathematical superposition or resolution for different color responses. This corollary provides the quantitative association for different response mechanisms of reflection colors.

2.2. Synthetic CCs and polarization-separated CCs are collinear.

In the CCs system, the slope functions of the two lines restricted by the synthetic CCs and polarization-separated CCs are defined as $k_1 = \frac{y - y_p}{x - x_p}$ (syn-p) and $k_2 = \frac{y - y_s}{x - x_s}$ (syn-s). Subsequently, substituting equations (4) and (5), the slope functions can be expanded as:

$$k_1 = \frac{Y_{syn}(X_p + Y_p + Z_p) - Y_p(X_{syn} + Y_{syn} + Z_{syn})}{X_{syn}(X_p + Y_p + Z_p) - X_p(X_{syn} + Y_{syn} + Z_{syn})} \quad (11)$$

$$k_2 = \frac{Y_{syn}(X_s + Y_s + Z_s) - Y_s(X_{syn} + Y_{syn} + Z_{syn})}{X_{syn}(X_s + Y_s + Z_s) - X_s(X_{syn} + Y_{syn} + Z_{syn})}. \quad (12)$$

Due to the arithmetical averaging properties of $T_{v\text{-}syn} = (T_{v\text{-}p} + T_{v\text{-}s})/2$ verified by corollary 2.1 above; equations (11) and (12) can be simplified and simultaneously exhibit an identical relation as follows:

$$k_1 = k_2 = \frac{Y_pX_s + Y_pZ_s - Y_sX_p - Y_sZ_p}{X_pY_s + X_pZ_s - X_sY_p - X_sZ_p} = \frac{Y_p(X_s + Z_s) - Y_s(X_p + Z_p)}{X_p(Y_s + Z_s) - X_s(Y_p + Z_p)}. \quad (13)$$

Identical slope and intersection (synthetic CCs) further demonstrate the collinearity of CCs. This means that the corresponding CCs of synthesis, s-polarization and p-polarization are collinear for an arbitrary incident angle θ and a multi-layer dielectric structure. To sum up, this corollary provides an effective criterion for determining the relative spatial position of polarized CCs; that is, collinearity of CCs. Furthermore, it indicates that the color response of an object can be obtained from the linear superposition of two kinds of polarizations.

2.3. Mathematic relation of tristimulus values is constant as $T_{v\text{-}s} > T_{v\text{-}p}$.

For common dielectric multi-layer films (non-magnetic and without surface plasmon resonance effects), longer transmission distance and a gradually non-parallel relation of the electric field (E) component to the incident interface render reflectivity enhanced (s-polarization, R_s) and reduced (p-polarization, R_p), respectively [17]. In particular, due to inconsonant trough-shifts between s-polarization and p-polarization, a small anomalous mathematic relation of polarization-separated spectral reflectance $R_s < R_p$ occurs around the interference wavelength at a certain incident angle θ. But beyond that, this relative relation can be expressed generally as $R_s > R_p$ [18, 19]. So, for visible broadband 380–780 nm, the constant mathematic relation can be derived as follows:

$$100\frac{\int_\lambda S(\lambda)R_s(\lambda)\bar{x}(\lambda)\mathrm{d}\lambda}{\int_\lambda S(\lambda)\bar{y}(\lambda)\mathrm{d}\lambda} > 100\frac{\int_\lambda S(\lambda)R_p(\lambda)\bar{x}(\lambda)\mathrm{d}\lambda}{\int_\lambda S(\lambda)\bar{y}(\lambda)\mathrm{d}\lambda}. \quad (14)$$

Therefore, $X_s > X_p$ is directly verified. It can be also generalized to $Y_s > Y_p$ (or $Y_s\% > Y_p\%$) and $Z_s > Z_p$. This corollary applies to assisted verification and a semi-quantitative calculation for the mathematic relation of tristimulus values; that is, the constant mathematic relation $T_{v\text{-}s} > T_{v\text{-}p}$.

For practical application, it can be interpreted that there certainly exists higher luminance and greater contribution of three-primary colors for s-polarization than those of p-polarization.

2.4. Synthetic CCs are partial to s-polarized CCs

Based on the collinearity of the chromaticity coordinates derived from corollary 2.2, the complicated derivation procedure about the spatial relationship of polarized CCs can be simplified to a single distance calculation of abscissa ($|x_s–x_{syn}|$ and $|x_p–x_{syn}|$) or ordinate ($|y_s–y_{syn}|$ and $|y_s–y_{syn}|$). This means that a numerical comparison between $d_{s\text{-}syn}$ ($=\sqrt{(x_s - x_{syn})^2 + (y_s - y_{syn})^2}$, the distance from the synthetic CCs to s-polarized CCs) and $d_{p\text{-}syn}$ ($=\sqrt{(x_p - x_{syn})^2 + (y_p - y_{syn})^2}$, the distance from the synthetic CCs to p-polarized CCs) can be determined by the comparison result between $d(x)_{s\text{-}syn}$ ($=|x_s–x_{syn}|$, x-distance from the synthetic CCs to s-polarized CCs) and $d(x)_{p\text{-}syn}$ ($=|x_p–x_{syn}|$, x-distance from synthetic CCs to p-polarized CCs). So we have defined the differential function as follows:

$$\Delta = d(x)_{p-syn} - d(x)_{s-syn} = |x_p–x_{syn}| - |x_s–x_{syn}|. \quad (15)$$

Based on a different spatial relationship (x_s and x_p), it can be rewritten as the following piecewise functions:

$$\begin{cases} 2x_{syn} > (x_s + x_p) & x_s > x_p \\ 2x_{syn} = (x_s + x_p) & x_s = x_p, \\ 2x_{syn} < (x_s + x_p) & x_s < x_p \end{cases} \quad (16)$$

where x_s, x_p and x_{syn} are a positive number due to the CIE 1931 standard. For the condition of $x_s > x_p$, by substituting equations (4), (5) and (8)–(10) into equation (16) in succession, we can directly obtain the equivalent equations as follows:

$$\frac{2(X_s + X_p)}{X_s + X_p + Y_s + Y_p + Z_s + Z_p} > \left(\frac{X_s}{X_s + Y_s + Z_s} + \frac{X_p}{X_p + Y_p + Z_p}\right) \quad (17)$$

$$\begin{aligned} &2(X_s + X_p)(X_s + Y_s + Z_s)(X_p + Y_p + Z_p) \\ &- (X_s + X_p + Y_s + Y_p + Z_s + Z_p)X_s \\ &\times (X_p + Y_p + Z_p)X_p(X_s + Y_s + Z_s) > 0. \end{aligned} \quad (18)$$

Then, after multiple decompositions and syntheses, the complex polynomial above is finally resolved as:

$$\begin{aligned} &(X_sY_p + X_sZ_p - X_pY_s - X_pZ_s)[(X_s - X_p) \\ &+(Y_s - Y_p) + (Z_s - Z_p)] > 0. \end{aligned} \quad (19)$$

Due to the constant mathematic relation $T_{v\text{-}s} > T_{v\text{-}p}$ derived in corollary 3, equation (19) can be subtly simplified as:

$$X_s(X_p + Y_p + Z_p) - X_p(X_s + Y_s + Z_s) > 0.$$

Ultimately, an obvious equivalent equation is established that exactly echoes the precondition $x_s > x_p$:

$$\frac{X_s}{X_s + Y_s + Z_s} > \frac{X_p}{X_p + Y_p + Z_p} \Leftrightarrow x_s > x_p.$$

The same derivation can be directly applied for the condition of $x_s < x_p$ and $x_s = x_p$. Therefore, a definite mathematic relation $\Delta > 0$ has been successfully derived and verified, which can be further retrocalculated as: $d_{p\text{-}syn} > d_{s\text{-}syn}$. The corollary applies to assisted verification and qualitative calculation for the relative spatial position of CCs; that is, synthetic CCs partial to s-polarized CCs. This interesting spatial relationship further boils down to a gradually widening gap between the increasing total $R_s(\lambda)$ and decreasing total $R_p(\lambda)$, which appears intuitively as greater homoplasy of macroscopic color feedback to the corresponding s-polarization.

3. Experimental results and discussion

A conventional colorimeter is unable to dabble in oblique incidence; so indirect measurement was utilized that included pre-stage reflectance $R(\lambda)$ measurement and post-stage chromaticity calculation (CCs, LF and T_v).

Reflection spectra corresponding to representative θ (45°, 60° and 75°) and thickness-tunable d_L (30, 60 and 90 nm) were measured by a Mueller matrix spectroscopic ellipsometer (ME-L) in the wavelength range of 380–780 nm [20]. Due to the non-transparency of the designed structure in a visible range, influence from the lower interface of the K9 optical substrate can be eliminated without acid corrosion or rough sanding treatment. A pre-measuring procedure was performed so that SiO_2 film (25 nm) was chosen as a reference to calibrate parameters. As shown in figure 3(a)–(i), different reflection spectra $R(\lambda)$ are obviously polarization-separated into symmetrical s-$R(\lambda)$ and p-$R(\lambda)$, which are converted from spectral intensity I based on standard SiO_2. In addition, following the increase of d_L and θ, troughs of interference shift towards long-wavelength and the polarization-separated degree of $R(\lambda)$ gradually grows larger, respectively. It can be found that s-$R(\lambda)$ is generally greater than p-$R(\lambda)$, except for a tiny abnormality occurring around the interference wavelength λ_i. As the root cause of corollary 2.1–2.4, this phenomenon is mainly caused by inconsonant transmission performances (transmission distance and relative direction to surface) of the E component between s-polarization and p-polarization, which further leads to the deviation of trough-shifts in the whole range of 380–780 nm.

Post-stage chromaticity calculation can be generalized into the transformation from pre-stage $R(\lambda)$ to intrinsic color parameters (CCs, LF and T_v), which have been explicitly defined in equations (1)–(5). As listed in tables 1–3, T_v (X, Y and Z) and CCs ((x, y)) corresponding to all combinations of d_L and θ have been sequentially calculated, which can be divided into three categories: synthesis, s mode and p mode. Inductive corollary 2.1 and 2.3 are quantificationally verified by relevant data, which can be generalized as the general expressions $T_{v\text{-}synthesis} = (T_{v\text{-}s} + T_{v\text{-}p})/2$ (or LF relation:

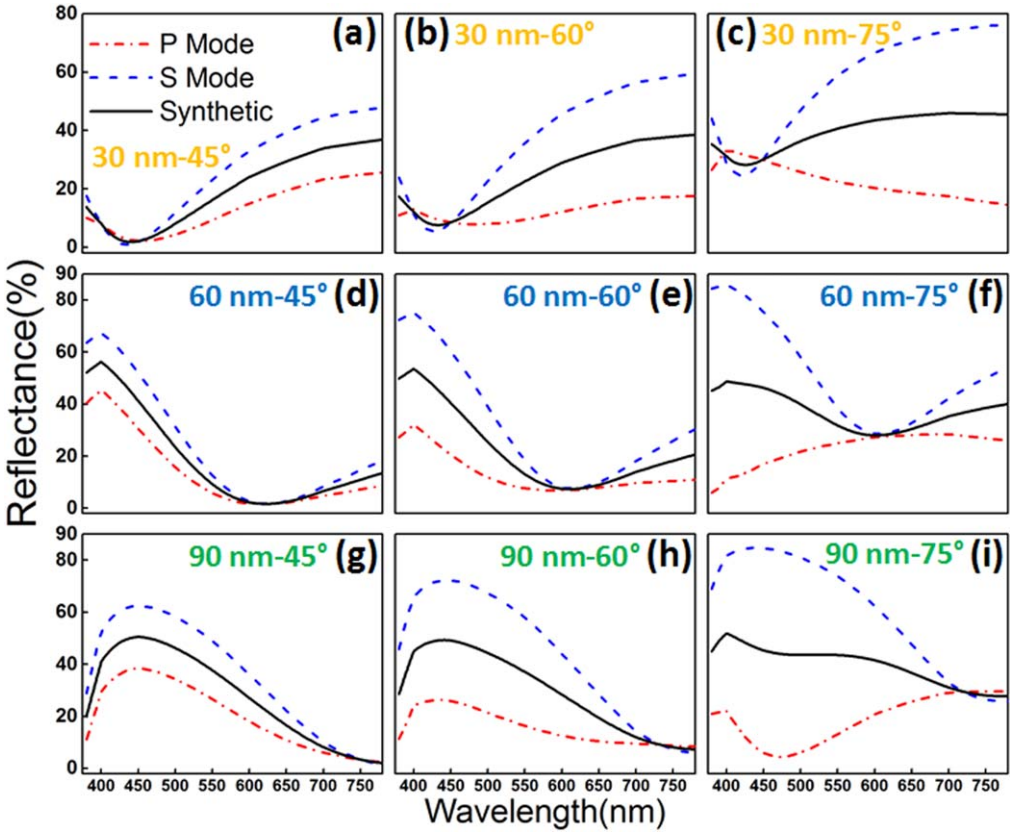

Figure 3. Measured polarization-separated reflection spectra for different combinations of θ (=45°, 60° and 75°) and dL (=30, 60 and 90 nm).

Table 1. Different experimental parameters of CIE 1931 for $d_L = 30$ nm at various θ 45°, 60° and 75°.

θ (deg)	Mode	X	Y	Z	(x, y)
45°	synthesis	17.5	16.2	3.5	(0.471, 0.436)
	p mode	11.1	9.7	3.2	(0.461, 0.406)
	s mode	24.0	22.8	3.8	(0.475, 0.451)
60°	synthesis	22.6	22.3	10.3	(0.410, 0.404)
	p mode	10.5	10.0	9.5	(0.352, 0.333)
	s mode	34.7	34.7	11.1	(0.432, 0.431)
75°	synthesis	38.2	40.1	33.1	(0.343, 0.360)
	p mode	21.4	22.9	31.7	(0.282, 0.301)
	s mode	55.1	57.3	34.5	(0.375, 0.390)

Table 2. Different experimental parameters of CIE 1931 for $d_L = 60$ nm at various θ 45°, 60° and 75°.

θ (deg)	Mode	X	Y	Z	(x, y)
45°	synthesis	11.2	11.9	43.1	(0.169, 0.179)
	p mode	8.2	8.0	32.1	(0.170, 0.166)
	s mode	14.2	15.7	54.4	(0.168, 0.187)
60°	synthesis	14.8	15.5	42.6	(0.203, 0.213)
	p mode	9.5	9.0	21.9	(0.235, 0.223)
	s mode	20.1	22.1	63.2	(0.191, 0.209)
75°	synthesis	31.1	33.3	48.9	(0.274, 0.294)
	p mode	23.4	24.6	18.2	(0.353, 0.372)
	s mode	38.7	41.9	79.6	(0.242, 0.262)

$Y_{\text{synthesis}}\% = (Y_s\% + Y_p\%)/2)$ and $T_{\text{v-s}} > T_{\text{v-p}}$, respectively. In addition, as depicted in figure 4, all the combined calculations and point tracing of CCs have been accomplished. In order to clearly discern the independent distribution laws of CCs, locally amplified chromaticity diagrams are specifically provided in the insets of figure 4(a)–(c), where the color information corresponds to tables 1–3, respectively. The expected collinearity and the constant relative spatial relation can be intuitively observed, which successfully verify the correctness of corollary 2.2 ($k_{\text{s-synthesis}} = k_{\text{p-synthesis}}$) and 2.4 ($d_{\text{p-synthesis}} > d_{\text{s-synthesis}}$). Slight deviations are totally acceptable due to the inevitable errors from the measuring process of $R(\lambda)$ and approximate treatment of data.

Table 3. Different experimental parameters of CIE 1931 for $d_L = 90$ nm at various θ 45°, 60° and 75°.

θ (deg)	Mode	X	Y	Z	(x, y)
45°	synthesis	31.2	36.6	52.8	(0.259, 0.304)
	p mode	21.9	26.0	39.8	(0.250, 0.296)
	s mode	40.5	47.3	65.7	(0.264 0.308)
60°	synthesis	31.7	36.3	51.7	(0.265, 0.303)
	p mode	15.0	16.7	27.0	(0.255, 0.285)
	s mode	48.5	55.9	76.3	(0.268, 0.309)
75°	synthesis	40.1	42.8	49.0	(0.304, 0.324)
	p mode	15.9	13.7	7.9	(0.424, 0.364)
	s mode	64.3	71.9	90.1	(0.284, 0.318)

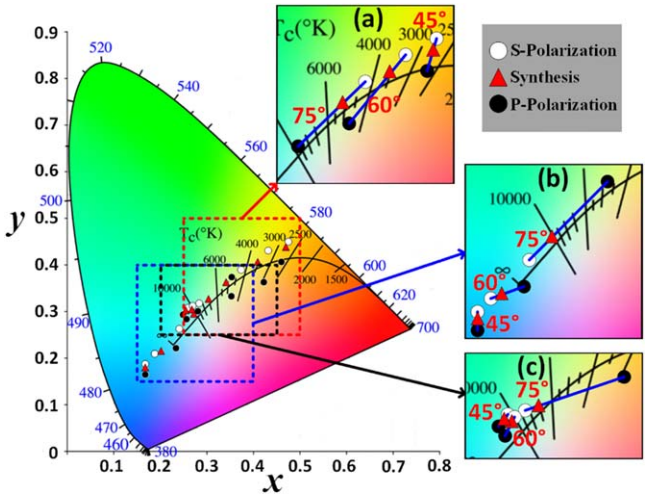

Figure 4. Experimental CCs of synthesis (red), s-polarization (white) and s-polarization (black) corresponding to different θ (=45°, 60° and 75°) and d_L (=30, 60 and 90 nm); locally amplified insets: (a) d_L = 30 nm, (b) d_L = 60 nm and (c) d_L = 90 nm.

4. Conclusions

In conclusion, we have firstly proposed and deduced four corollaries about polarization-separated color attributes for the structure $L/(Ge/ZnS)^3$. These corollaries have been subsequently corroborated by analysis based on rigorous mathematical derivation and experiment, which establish the quantitative relations among different color components of synthesis, s-polarization and p-polarization. Specifically, for LF and T_v, corollaries can be generalized into arithmetical averaging properties $T_{v\text{-synthesis}} = (T_{v\text{-s}} + T_{v\text{-p}})/2$ (or $Y_{synthesis}\% = (Y_s\% + Y_p\%)/2$) and constant mathematic relation $T_{v\text{-s}} > T_{v\text{-p}}$; for CCs, corollaries also can be concisely described as collinearity ($k_{s\text{-synthesis}} = k_{p\text{-synthesis}}$) and synthetic partial to s-polarization ($d_{p\text{-synthesis}} > d_{s\text{-synthesis}}$). These mathematical laws possess an obvious universality for common dielectric multi-layer structures without any restrictions from the intrinsic parameters of materials and structure. Therefore, inductive corollaries will certainly provide an effective mathematical basis and extend the theorem system for polarization-separated color attributes for multi-layer dielectric structures.

Acknowledgments

This work is supported by the National Natural Science Foundation of China (61701185 and 61801186), the China Postdoctoral Science Foundation funded Project (2017M622444, 2018T110764 and 2018M630859).

ORCID iDs

Xian Wang https://orcid.org/0000-0002-5448-0607
Shiyuan Liu https://orcid.org/0000-0002-0756-1439

References

[1] Noh J H, Im S H, Heo J H, Mandal T N and Seok S I 2013 Chemical management for colorful, efficient, and stable inorganic-organic hybrid nanostructured solar cells *Nano Lett.* **13** 1764–9
[2] Zhao Y, Xie Z, Gu H, Zhu C and Gu Z 2012 Bio-inspired variable structural color materials *Chem. Soc. Rev.* **41** 3297–317
[3] Vashistha V, Vaidya G, Hegde R S, Serebryannikov A E, Bonod N and Krawczyk M 2017 All-dielectric metasurfaces based on cross-shaped resonators for color pixels with extended gamut *ACS Photon.* **4** 1076–82
[4] Wang H, Wang X, Yan C, Zhao H, Zhang J, Santschi C and Martin O J F 2017 Full color generation using silver tandem nanodisks *ACS Nano* **11** 4419–27
[5] Pursiainen O L J, Baumberg J J, Winkler H, Viel B, Spahn P and Ruhl T 2007 Nanoparticle-tuned structural color from polymer opals *Opt. Express* **15** 9553–61
[6] Qi D, Cheng Y, Wang X, Wang F, Li B and Gong R 2017 Multi-layer composite structure covered polytetrafluoroethylene for visible-infrared-radar spectral compatibility *J. Phys. D: Appl. Phys.* **50** 505108
[7] Fang Z H, Punckt C, Leung E Y, Schniepp H C and Aksay I A 2010 Tuning of structural color using a dielectric actuator and multifunctional compliant electrodes *Appl. Opt.* **49** 6689–96
[8] Chung K *et al* 2012 Flexible, angle-independent, structural color reflectors inspired by morpho butterfly wings *Adv. Mater.* **24** 2375–9
[9] Cheng F, Gao J, Luk T S and Yang X 2015 Structural color printing based on plasmonic metasurfaces of perfect light absorption *Sci. Rep.* **5** 11045
[10] Qi D, Chen F, Wang X, Luo H, Cheng Y, Niu X and Gong R 2018 Effective strategy for visible-infrared compatible camouflage: surface graphical one-dimensional photonic crystal *Opt. Lett.* **43** 5323–6
[11] Li Z, Butun S and Aydin K 2015 Large-area, lithography-free super absorbers and color filters at visible frequencies using ultrathin metallic films *ACS Photon.* **2** 183–8
[12] Wu Z, Lee D, Rubner M F and Cohen R E 2007 Structural color in porous, superhydrophilic, and self-cleaning SiO_2/TiO_2 Bragg stacks *Small* **3** 1445–51
[13] Querry M 1987 Optical constants of minerals and other materials from the millimeter to the ultraviolet *Contractor Report* CRDEC-CR-88009 Chemical Research Development and Engineering Center Aberdeen Proving Ground
[14] Li H H 1980 Refractive index of silicon and germanium and its wavelength and temperature derivatives *J. Phys. Chem. Ref. Data* **9** 561–658
[15] Wyszecki G and Stiles W S 1982 *Color Science: Concepts and Methods, Quantitative Data and Formulae* (New York: Wiley)
[16] Centurioni E 2005 Generalized matrix method for calculation of internal light energy flux in mixed coherent and incoherent multilayers *Appl. Opt.* **44** 7532–9
[17] Liu J, Liu N, Li J, Li X and Huang J 2012 Enhanced absorption of graphene with one-dimensional photonic crystal *Appl. Phys. Lett.* **101** 052104
[18] Joerger R, Forcht K, Gombert A, Köhl M and Graf W 1997 Influence of incoherent superposition of light on ellipsometric coefficients *Appl. Opt.* **36** 319–27
[19] Kjornrattanawanich B, Bajt S and Seely J F 2004 $Mo/B_4C/Si$ multilayer-coated photodiode with polarization sensitivity at an extreme-ultraviolet wavelength of 13.5 nm *Appl. Opt.* **43** 1082–90
[20] Liu S, Chen X and Zhang C 2015 Development of a broadband Mueller matrix ellipsometer as a powerful tool for nanostructure metrology *Thin Solid Films* **584** 176–85